Journal Name

ARTICLE

Co-percolation To Tune Conductive Behaviour in Dynamical Metallic Nanowire Networks

Received 00th January 20xx,
Accepted 00th January 20xx

DOI: 10.1039/x0xx00000x

www.rsc.org/

J. A. Fairfield[a,c,†], C. G. Rocha[b,c], C. O'Callaghan[b,c], M. S. Ferreira[b,c] and J. J. Boland[a,c,*]

Nanowire networks act as self-healing smart materials, whose sheet resistance can be tuned via an externally applied voltage stimulus. This memristive response occurs due to modification of junction resistances to form a connectivity path across the lowest barrier junctions in the network. While most network studies have been performed on expensive noble metal nanowires like silver, networks of inexpensive nickel nanowires with a nickel oxide coating can also demonstrate resistive switching, a common feature of metal oxides with filamentary conduction. However, networks made from solely nickel nanowires have high operation voltages which prohibit large-scale material applications. Here we show, using both experiment and simulation, that a heterogeneous network of nickel and silver nanowires allows optimization of the activation voltage, as well as tuning of the conduction behavior to be either resistive switching, memristive, or a combination of both. Small percentages of silver nanowires, below the percolation threshold, induce these changes in electrical behavior, even for low area coverage and hence very transparent films. Silver nanowires act as current concentrators, amplifying conductivity locally as shown in our computational dynamical activation framework for networks of junctions. These results demonstrate that a heterogeneous nanowire network can act as a cost-effective adaptive material with minimal use of noble metal nanowires, without losing memristive behaviour that is essential for smart sensing and neuromorphic applications.

Introduction

Metallic nanowire networks are flexible, electrically active materials with great promise for use as transparent conductors,[1–3] solar cells,[4–6] fuel cells,[7–9] generators,[10] stretchable[11–15] and sensor[16,17] devices. These networks typically consist of randomly dispersed metallic nanowires coated with an active dielectric shell, either as the result of oxidation or due to passivation chemistry necessary to prevent flocculation in solution. The presence of this outer shell results in the emergence of new and intriguing electronic properties. For example, networks made of polymer-coated silver nanowires with high aspect ratio and modified junction resistance are known to produce the lowest sheet resistances,[1,17–22] whereas oxide-coated nickel nanowire networks demonstrate electrically-induced programmability.[23] Nanowire networks comprised of either material act as memristive systems whose sheet resistance (R_s) depends on the electrical measurement history of the network,[24] stemming from the collective response of nanowire-nanowire junctions that serve as memristive units.

In these electrically stressed networks, it is critical to control the activation voltage of the sample (V_{on}), i.e. the threshold voltage at which a conducting percolative path is formed across the network and current can begin to flow through the material. The reduction of V_{on} is an important challenge, especially for large area networks whose memristive response can only be activated by extremely high voltages. For instance, square Ni nanowire networks with lateral dimensions (d) ranging from 100-200 μm can exhibit activation voltage values ranging 100-200 V.[18] We have previously shown an efficient strategy to tune activation voltages and sheet resistances of nanowire network materials, by altering the shape of the electrodes to lower V_{on} as well as the sheet resistance of the network by over 40%.[25] The conducting features of nanowire networks can also be controlled using a wide range of experimental procedures such as application of heat,[2,3,26] light,[27,28] or compression,[29] however many of these approaches remove the evolutionary behavior required to create programmable materials and neuromorphic circuits.[30] New approaches are needed that do not sacrifice the characteristic synthetic memory of nanowire networks, to enable larger networks to manifest memristive response at low voltages.

[a] School of Chemistry, Trinity College Dublin, Dublin 2, Ireland.
[b] School of Physics, Trinity College Dublin, Dublin 2, Ireland.
[c] Centre for Research on Adaptive Nanostructures and Nanodevices (CRANN), Trinity College Dublin, Dublin 2, Ireland.
†Present address: School of Physics, National University of Ireland Galway, University Road, Galway, Ireland.
*Author to whom correspondence should be addressed: jboland@tcd.ie
Electronic Supplementary Information (ESI) available: Table of nanowire densities, comparison of arithmetic versus geometric mean for Ni-Ag nanowire junctions, screenshots and animated videos of dynamical activation of nanowire networks, and comparison of capacitance contrast results. See DOI: 10.1039/x0xx00000x

In this work we show that synthesizing hybrid nanowire networks composed of a mix of Ag and Ni nanowires is an effective strategy for controlling the voltage needed for both activation and for the onset of memristive hysteresis loops. We demonstrate that relatively small percentages of Ag nanowires are needed to effectively tune the conducting features of the samples, even in sparse networks. Simulations support this observation and show that hybrid Ni/Ag networks are electrically activated at a considerably lower voltage than pure Ni ones. However, above a certain density threshold the addition of Ag nanowires saturates the system, resulting in a percolative silver network which bypasses the Ni channels. Remarkably, sufficiently large area Ni/Ag networks could be electrically activated and demonstrated memristive behaviors which are normally not achieved for Ni-only networks of same sizes. While co-percolation[31] has been previously demonstrated in conducting films of Ag nanowires and carbon nanotubes,[32–34] this is the first demonstration of a co-percolating silver and nickel network, and the first co-percolating network to demonstrate resistive switching. By expanding our previous computational network model to include dynamical activation, we also demonstrate the importance of Ag nanowires in controlling and modifying local current connectivity. The co-percolating network fabrication approach described is considerably simpler to implement in comparison to competing hybrid networks with layers of different metals which require many processing steps for synthesis or fabrication.[35,36] These results enable efficient use of noble metal nanowires, by showing that minimum amounts of Ag embedded in a Ni nanowire network can improve operational parameters. Moreover, the electrical performance of nanowire networks can be dramatically improved by adding small amounts of expensive noble metal nanowires, while retaining memristive behavior needed for smart sensing and neuromorphic computation.

Results and Discussion

Experiments. Nanowire networks were fabricated by spraying a mixture of Ni and Ag nanowires, following a previously established facile method applicable to any substrate.[19] First, the nanowire spray solution was made by mixing commercially obtained solutions in isopropanol of Ag nanowires (Seashell Tech, length 10 ± 2 µm, diameter 60 ± 10 nm) and Ni nanowires (Nanomaterials.it, length 8 ± 2 µm, diameter 35 ± 10 nm). The Ag nanowires have a surface coating of polyvinylpyrrolidone (PVP) which is 1-2 nm thick, and the Ni nanowires have a native self-limiting surface oxide which is 4-5 nm thick, as measured by transmission electron microscopy. Both coatings act as barriers to conduction which can be modified by electrical stress, an effect which has been extensively studied in single-species nanowire networks.[18,23,25] The combined Ni/Ag nanowire solution is then spray deposited onto a silicon wafer with a 300 nm thick thermal oxide coating, using an artist's spray gun mounted on an automated x-y translation stage. This approach yields a very even dispersion of randomly oriented nanowires on the substrate,[19] which can then be electrically contacted and measured. Electrodes were then fabricated by electron beam evaporation of 5 nm of Ti and 85 nm of Au through a shadow mask which defined the electrode shapes on the substrate.

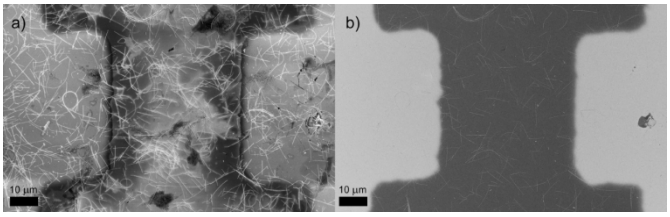

Figure 1: A nanowire network with 50 µm electrode separation is shown in two scanning electron micrographs, through (a) an in-lens detector and (b) an energy-selective backscatter detector. In both images, the metal electrodes where probes contacted the nanowire network are visible as rectangular blocks on the left and right sides. While the in-lens detector shows surface morphology well, in the energy-selective backscatter image the silver nanowires appear brighter than the nickel nanowires, showing the network has 70% Ni and 30% Ag nanowires.

After spraying, nanowire films were characterized in a scanning electron microscope (SEM). An energy-selective backscattered (ESB) detector showed the silver nanowires as brighter than the nickel nanowires, due to the higher atomic number of Ag, enabling the exact ratio of nickel to silver nanowires to be determined for each device. Figure 1 shows SEM and ESB images for a network with a density of 0.2 NW/µm^2 and a composition of 70/30 Ni/Ag. Electrodes are visible to either side, defining a 50 x 50 µm active device area. All networks studied were approximately square in shape, with a calculated optical transmission of 94-95%.[37]

Electrical measurements were carried out in a probe station, with the voltage applied and current read out by a Keithley 4200-SCS. Devices were first measured under a compliance current of 10 µA, to limit the current through the device during activation. Before electrical stressing, each junction in the network is capacitive and acts as a barrier to conduction. Increasing the voltage applied causes individual junctions to become resistive either through breakdown of the polymer capping layer on Ag wires or through the growth of a metallic filament through the native oxide coating on Ni wires. Filamentary conduction is the mechanism behind a well-studied effect in metal oxides called resistive switching (RS).[38,39] At some critical activation voltage, a conducting path is formed connecting these resistive junctions, and current flows through the network. The compliance current prevents runaway activation and Joule heating from melting the nanowires or junctions, after which the voltage is swept back to zero and the compliance current removed. The voltage is then swept again to observe the current-voltage (I-V) characteristics of the device. The three types of I-V behavior observed in these nanowire networks are shown in Figure 2, for a variety of network sizes.

The addition of silver nanowires changes the observed I-V properties of the nanowire networks, depending on the percentage of Ag nanowires compared to Ni. Figure 2(a) shows

resistive switching in a 68/32 Ni/Ag nanowire 50 x 50 µm device which has already been activated via an I-V sweep with a 10 µA current compliance. Resistive switching would not normally be observed in such a large network of nickel only nanowires, but the addition of silver reduces the number of Ni/Ni junctions present in a conduction path, preserving the resistive switching even for larger network sizes[23]. In Figure 2(b), a 200 µm nickel-only network after activation displays an intermediate behavior with hysteresis loops which contain resistive switching between discrete levels. Finally, in Figure 2(c) purely memristive behavior is observed in a 1 mm 93/7 Ni/Ag network, with hysteresis loops which retain no trace of resistive switching. This size of network was previously not reliably operable for nickel only networks, because of the large voltages required to form conducting filaments through such a large number of Ni/NiO/Ni junctions.

The I-V behavior of multiple Ni nanowire networks and hybrid Ni/Ag networks of distinct sizes was analyzed and their behaviors were classified as either resistive switching (RS), memristive loops (MR), or a combination of the two (SD loops). The results are presented in Table 1. The addition of silver nanowires also changes the voltage at which activation occurs. Activation voltages were measured for nanowire network devices with varying ratios of Ni/Ag nanowires, in which these three types of I-V curve—resistive switching, semi-digital loops, and memristive loops—were observed. The voltages are normalized with respect to the total nanowire density of the network as detailed in the Supplementary Information, Table S1. This is necessary to suppress the effect of fluctuations in the wire densities of the various network samples that are known to affect the absolute value of the activation voltages.[18]

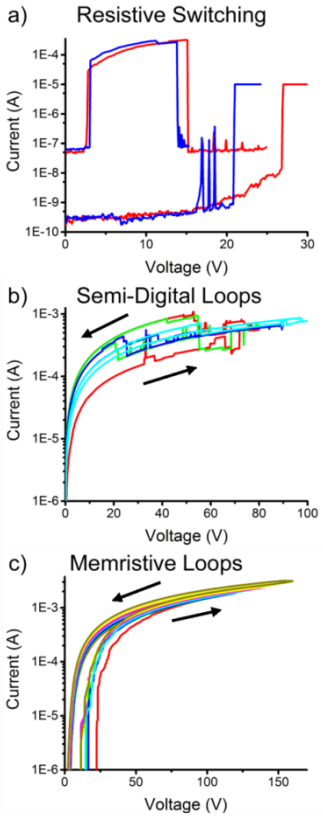

Figure 2: Types of I-V behavior observed in nanowire networks. (a) On/off resistive switching observed in a 50 x 50 µm device with Ni/Ag proportions of 68/32. (b) Semi-digital hysteresis loops observed in a 200 x 200 µm nickel-only network. (c) Memristive evolutionary loops observed in a 1 x 1 mm Ni/Ag 93/7 device. In all devices the red traces were measured first, and arrows indicate hysteresis direction.

Table 1: Evolutionary behavior in nanowire networks of varying compositions of Ni/Ag. RS refers to resistive switching with clear off state, MR refers to memristive loops and SD refers to the combination of RS and MR behaviours (semi-digital). Some networks could not be activated and remained in the off state.

Network Size (µm)	*Ni/Ag 100/0*	*Ni/Ag 93/7*	*Ni/Ag 85/15*	*Ni/Ag 70/30*	*Ni/Ag 68/32*
50	RS	RS	RS	RS	RS
100	MR	SD	RS	MR	RS
200	MR	MR	RS	MR	MR
500	Off	SD	Off	SD	MR
1000	Off	MR	Off	MR	MR

The weight factor is defined as n_{ref}/n_{real}, where n_{real} is the experimental wire density found on Table S1 and n_{ref} the reference wire density established to be 0.25 NW/µm^2 which is the average wire density of all studied samples. Nanowire densities ranged from 0.19-0.30 NW/µm^2 and were measured using SEM. The results are shown in Figure 3 which depicts V_{on} as a function of Ag nanowire density (n_{Ag}) for samples of distinct sizes. The estimated error is ±6 V for the 50 x 50 µm networks, ±8 V for the 100 x 100 µm networks, ±10 V for the 200 x 200 µm networks, and ±40 V for the 500 x 500 µm and 1000 x 1000 µm networks. Despite the notable dispersion in V_{on}, the addition of silver nanowires onto the Ni frame reduces the activation voltage for the majority of network samples. Remarkably, pure Ni networks of dimensions above 500 x 500 µm could not even be activated (no data points in Figure 3 at n_{Ag} = 0 for the two largest samples). However, after adding Ag nanowires to these large networks, they could be activated and operated normally, demonstrating that Ag nanowires facilitate the activation of the Ni network due to the lower amount of energy required for breakdown of polymer coating on the Ag nanowires compared to the barrier to metallic filament formation in the oxide coating on the nickel nanowires.[18]

Larger device areas which cannot be activated as nickel-only nanowire networks can exhibit memristive behavior when particularly small quantities of silver nanowires are added. The addition of silver nanowires also increases the device size at which resistive switching in predominantly nickel nanowire networks can be observed, a potentially useful outcome for creating large-scale resistive switching materials. Devices which displayed memristive loops also had small nonlinearities around low voltages, in line with recent reports and suggesting the filaments formed in the nanowire junctions are truly metallic.[40] These nonlinearities are expected given that most of the junctions will be Ni/Ni, with relatively few Ni/Ag junctions containing both an oxide and a polymer capacitive layer, and

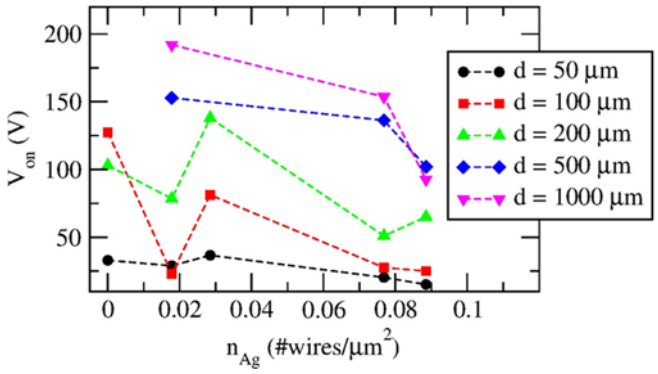

Figure 3: Activation voltages (V_{on}) versus Ag nanowire density (n_{Ag}) measured for multiple nanowire networks of distinct dimensions d x d.

very few Ag/Ag junctions. Further addition of Ag nanowires will eventually lead to a network which is effectively no longer a heterogeneous Ni/Ag hybrid but a very sparse self-selected Ag nanowire network. As a result, much lower voltages will be required to activate such a network but there will be no resistive switching behaviour. Finding the optimal amount of silver to maximize the conduction responses of the networks is critical for technological use of heterogeneous networks, particularly to improve performance without eliminating resistive switching or adaptive behavior. For a quantitative approach to this issue, we turn to theoretical simulations of these networks, which allow us to tune more parameters than we can practically control in experimental measurements.

Simulations. Computational simulations were carried out on random network models made of sticks dispersed over an area of dimensions *d* x *d*. All simulated networks were square in shape with electrodes of width *d* being positioned at *x* = 0 and *x* = *d*. Networks with varied device sizes and nanowire densities (*n*) were created and mapped into a mathematical graph with wires represented by nodes and their intersections represented by edges. Two theoretical descriptions were used to characterize the transport properties of hybrid and pure Ni nanowire networks: (i) a voltage grid representation of resistors to describe static conducting features[41] of the networks and (ii) a second voltage grid representation of capacitors that can be subjected to breakdown. Formalism (ii) is particularly useful for tackling the dynamical activation of the networks and is explained in more detail below.

The sheet resistances of nanowire networks were obtained via an accurate charge transport picture developed by us, whose detailed explanation can be found in ref. 25. While previous simulation efforts in nanowire networks assumed that the junction resistance dominated,[42,43] in our formalism each wire is described by a multi-nodal representation which accounts for all characteristic resistances involved in the conducting process of a disordered network: the interwire junction resistance (R_j), as well as the inner-wire resistances given by $R_{in} = \rho\ell/A$ where ρ is the wire resistivity, ℓ its segment length and A the cross section area. For hybrid samples, the intrinsic characteristics of both Ag and Ni nanowires must be incorporated. The following experimentally determined values were used in the simulations: ρ_{Ag} = 22.6 ± 2.3 nΩm, ρ_{Ni} = 62 ± 19 nΩm, and the respective diameters are $D_{Ag} \approx 80$ nm and $D_{Ni} \approx 35$ nm. All wires were set with the same length of L = 7 μm. For statistical significance, an ensemble containing 25-50 representative nanowire network samples is analyzed by applying Ohm's and Kirchhoff's current laws[44] to determine the sheet resistance of each network with nanowire density *n*. Each sample has a total wire density of $n = n_{Ni} + n_{Ag}$ where n_{Ni} (n_{Ag}) specifies the number of Ni (Ag) nanowires per unit of area. For pure Ni nanowire networks, $n_{Ag} = 0$.

In addition to specifying intrinsic characteristics of the wires as above, we must characterize their interactions, by defining junction resistances for the three types of interwire junctions: Ag-Ag, Ni-Ni, and Ni-Ag. Our previous work showed that electrically stressed Ag-Ag junctions can reach resistances as low as ~11 Ω but a few junctions exhibit higher resistance values reaching 200-300 Ω.[45] Since networks addressed in this study were not subjected to the same level of electrical stress as conducted in ref. 29, we set all Ag-Ag junction resistances (R_j^{AA}) to the higher value. The Ni-Ni junction resistance (R_j^{NN}) was determined by fitting the calculated sheet resistance with the measured values taken for pure Ni nanowire networks. As expected for non-stressed Ni networks, the resulting R_j^{NN} extracted from the fitting is high, with an order of magnitude of 10^6 Ω. Finally we must characterize the Ni-Ag hybrid junction. A straightforward assumption is to define the hybrid junction

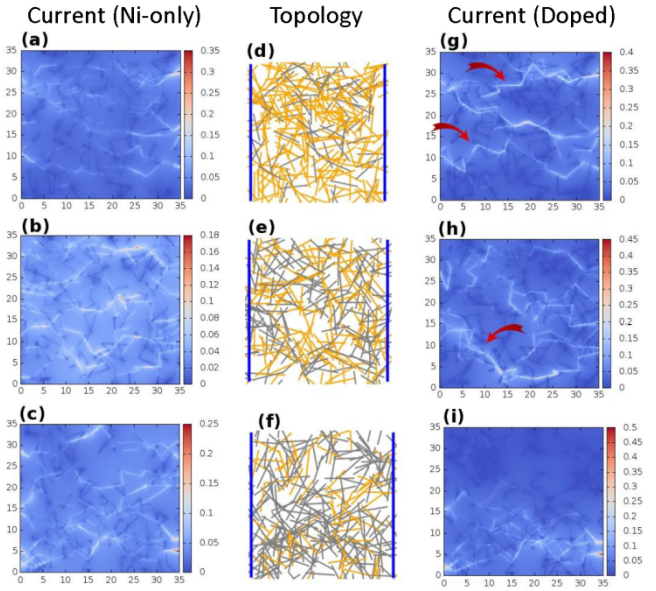

Figure 4: Current color maps calculated over each wire segment of pure Ni nanowire networks (left panels) and their corresponding hybrid versions (right panels). Middle panels depict the structural configuration of the analyzed networks: orange sticks represent Ni nanowires and grey ones correspond to Ag wires. Electrodes are represented by vertical blue sticks. Only the hybrid networks are displayed on the middle panels as their corresponding pure form follows the same topological structure except that all wires would be colored in orange. The Ni/Ag proportions of the hybrid nanowire networks are (d-g) 75/25%, (e-h) 50/50%, (f-i) 25/75%. The total wire density of all networks is fixed at n = 0.25 NW/μm^2 and the current color maps are expressed in arbitrary units. Arrows point at some regions where the current flow is redirected due to the presence of Ag wires.

resistance (R_j^{NA}) in terms of an arithmetic mean, $R_j^{NA} = (R_j^{NN} + R_j^{AA})/2$, or a geometric mean, $R_j^{NA} = \sqrt{(R_j^{NN}\, R_j^{AA})}$. Both definitions were tested and their respective outcomes were compared with experimental results (cf. Figure S1 in the Supplementary Information), with the geometric mean fitting more closely to experimental values for mixed Ni-Ag junctions.

Having defined all junction and wire resistances in heterogeneous Ni/Ag nanowire networks allows us to calculate the current flow through each wire segment and subsequently visualize this data in color map plots. These results are shown in Figure 4. The color maps visualize how the current is distributed across pure Ni networks, allowing comparison of current profiles with their corresponding hybrid versions generating by randomly replacing orange (Ni) wires with grey (Ag) wire to achieve the required composition. The maps indicate that the Ag wires work as "current concentrators", directing the current flow through the Ni network when their number density is low compared to that of the Ni wires. The arrows in the figure point to examples of this phenomenon. We note that the studied networks are relatively sparse (n = 0.25 NW/μm^2) and therefore, one can expect pronounced fluctuations in their transport response due to variations in local connectivity in these sparse networks.[25] For instance, the network with Ni/Ag = 25/75% behaves as a sparse Ag nanowire network with a particular connectivity pattern that favours the propagation of current across the lower section of the network.

To highlight the concentrating effect caused by Ag wires, we generated an ensemble containing over 100 network models of fixed wire density (n = 0.25 NW/μm^2) at distinct Ni/Ag concentrations. For all representative samples, we obtained the current flowing through each wire segment, then mapped the statistics of current events onto a histogram as shown in Figure 5. The number of wires carrying the highest current is greatest when the Ag wires are relatively dilute in the Ni network, confirming that optimal transport performance can be achieved using relatively small amounts of noble metals.

The computational description used so far can predict the static conducting properties of nanowire networks but is not sufficient to address their dynamical activation process. To simulate network activation, we employ a self-consistent capacitance-switching formalism that accounts for the gradual activation of the network upon application of a bias voltage. In this scheme, wires are treated as equipotential line segments and their connections described as binary capacitors. Depending on the voltage drop across the junction, the capacitor can be either non-activated (OFF-state) or activated (ON-state). A capacitor can transition from OFF→ON if the voltage drop across the junction is larger than its associated breakdown voltage (V_b), i.e. a given junction connecting a pair of wires (i,j) can be activated if $|V_i - V_j| \geq V_b$. The activation is characterized by a modification on the capacitance of the junction, in other words $C_{ij}^{OFF} \rightarrow C_{ij}^{ON}$ where C_{ij}^{OFF} is an estimated quantity determined uniquely by the characteristics of the wires and $C_{ij}^{ON} \rightarrow 0$. In order to avoid numerical inconsistencies C_{ij}^{ON} is set as a small tolerance value. The values

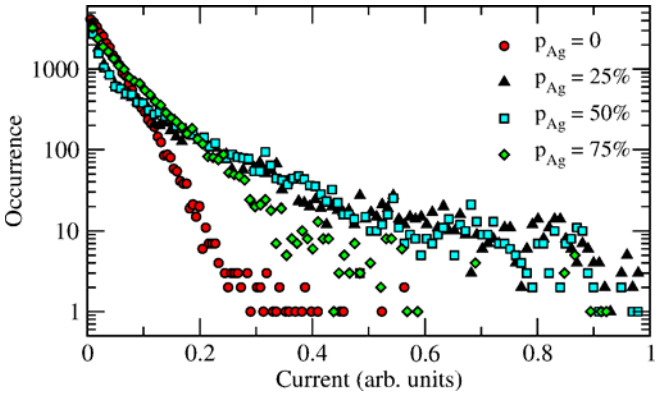

Figure 5: Histogram of current intensities per wire segment taken over 100 representative network samples with a fixed density of n = 0.25 NW/μm^2 and dimensions of 35 x 35 μm. The distributions are distinguished by their respective Ni/Ag proportions (p_{Ni}/p_{Ag}).

for C_{ij}^{OFF} are estimated by considering inter-wire junctions as parallel-plate capacitors with $C^{OFF} = \varepsilon_r A/4\pi h$ where ε_r is the relative static permittivity of the dielectric, A is the plate area, and h is their separation. This illustrative model is solely to identify qualitative trends, hence we use the estimated relative quantities: $\varepsilon_r^{PVP} \approx 2.5$, $h^{PVP} \sim 2 - 4\ nm$, $\varepsilon_r^{NiO} \approx 10.5$, $h^{NiO} \sim 4 - 10\ nm$. These assumptions give an OFF-state capacitance of polymer-coated Ag wires about six times larger than oxide-coated Ni nanowires, i.e. $C^{OFF}(Ag) = 6C^{OFF}(Ni)$. The corresponding breakdown voltage of the capacitor is assumed to be inversely proportional to C^{OFF} since $V_b = E_{ds}h$ where E_{ds} is the dielectric breakdown field strength.

The simulation begins by placing the whole capacitor network in contact with electrodes that source and drain a certain amount of charge Q, representing the charge that builds up due to the applied bias voltage. A capacitance matrix $\widehat{M}_c$ is built in the same fashion as described in ref. 14 and the potential on each wire (V) is obtained by solving the system of equations $\widehat{M}_c\widehat{V} = \widehat{Q}$. In contrast to the implementation used in ref. 14, charge on the electrodes is only incremented once all transition activity on the network ceases. If at least one junction had its state altered at a given charge Q, the capacitance matrix $\widehat{M}_c$ is modified and reinserted into $\widehat{M}_c\widehat{V} = \widehat{Q}$ without incrementing Q. This self-consistent procedure takes place until no further transitions occur, then charge on the electrodes is incremented by ΔQ.

Full animations of the dynamical activation predicted by our capacitance-switching model can be found in the Supplemental Information. Figure S2 in the Supplemental Information shows some snapshots of the dynamics for a pure Ni network and two hybrid networks with Ni/Ag = 95/5% and 75/25%. Charge is loaded on the electrodes until at a critical charge Q_{on} a path of activated junctions bridges them. The simulated activation path shows that the presence of Ag wires facilitates the activation of the network as $Q_{on}^{Ni} > Q_{on}^{hybrid}$, but also reveals that $Q_{on}^{95/5} < Q_{on}^{75/25}$, indicating that for relatively sparse networks the improvement of V_{on} does not depend only on the absolute concentration of Ag wires, but also on their position. This

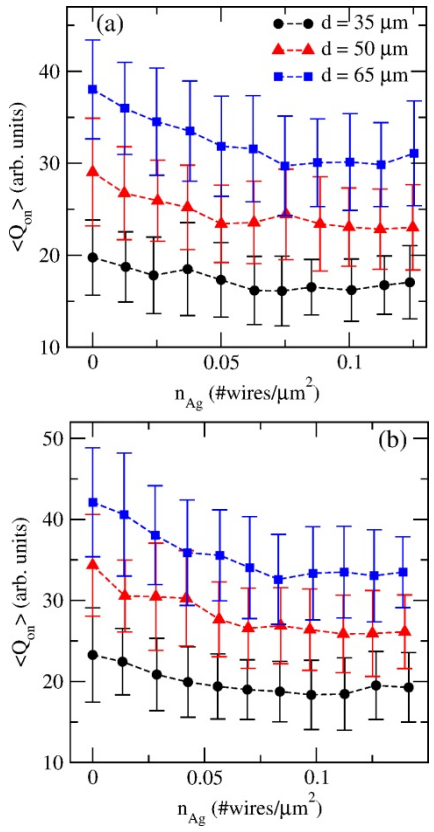

Figure 6: Average amount of charge required to establish a percolative path of activated junctions (<Q_{on}>) on Ni/Ag nanowire networks as a function of Ag wire density (n_{Ag}). Each data point is a result of statistical ensembles containing 50 representative networks of sizes *d* x *d* and fixed wire density of *n* = (a) 0.25 and (b) 0.28 NW/μm².

finding explains the seemingly unusual fluctuations observed in the measurements of V_{on} with respect to the concentration of Ag wires (cf. Figure 3). In general, optimal activation takes place when Ag wires are oriented transversely across the device as for instance where Ni/Ag = 95/5% (Figure S2 middle panels). In some configurations however, Ag nanowires are arranged in such a way that their presence is in fact a disturbance to activation, as for Ni/Ag = 75/25% (Figure S2 lower panels). This results in a more straightforward activation path for Ni/Ag = 95/5% whereas a bending path is formed for the higher concentration of Ag NWs with Ni/Ag = 75/25%.

Our capacitor-switching formalism was employed on an ensemble of network models with a fixed wire density *n* and distinct Ag concentrations. From the simulations, we obtained <Q_{on}> as a function of n_{Ag} for distinct network sizes *d* and these results are shown in Figure 6. The average value of Q_{on} is reduced as a result of adding Ag nanowires until n_{Ag} reaches a critical density n_c, however fluctuations occur due to the level of sparsity of the networks studied here. The percolation threshold density where the Ag sub-network spans the device, n_c, can be estimated through the formula $n_c L^2 = 5.63726$ derived numerically for an isotropic stick network[46]. For *L* = 7 μm, we obtain n_c = 0.11 Ag NW/μm², a rough threshold that establishes a crossover in the activation process of the hybrid networks. This threshold reveals that a significant reduction in the <Q_{on}> values of Ni nanowire networks of any size can occur when the concentration of Ag wires is in the range of n_c. The reduction in <Q_{on}> can be even more pronounced depending on the contrast in capacitance values used in the model. Figure S3 in the Supplementary Information compares the results shown in Figure 6 with the case where the capacitance contrast was artificially increased to $C^{OFF}(Ag) = 20C^{OFF}(Ni)$, confirming that co-percolative networks have improved electrical activation compared to single-metal nanowire networks.

As a result of the random nature of the network synthesis process, one cannot control where the Ag nanowires will sit on the Ni frame: they are spread throughout the entire network. Ideally, optimum activation of hybrid Ni/Ag nanowire networks could be achieved by depositing Ag wires in strategic positions across the network. From the computational point of view, one could suggest the use of graph algorithms targeting edge-connectivity augmentation (ECA) methods[47,48] which could in principle, determine a set of edges that could be manipulated in order to improve the connectivity of a graph. Unfortunately, ECA is impractical for the purpose of nanowire network activation since such phenomenon is fundamentally a dynamical process. By comparing the dynamical activation of a co-percolative network compared with the same network containing only Ni, our model proves in a quantitatively that the activation of Ni nanowire networks can be improved with the aid of Ag nanowires. On average, Q_{on} diminishes with the concentration of Ag nanowires, in particular for sufficiently large Ni networks which are the most challenging to activate.

Conclusions

We have conducted a systematic computational and experimental analysis of electrical behavior in metallic nanowire networks consisting of a small concentration of Ag wires within a Ni nanowire network. By creating nanowire networks of junctions with distinct filamentary characteristics, we have observed a rich transport scenario including resistive switching as well as memristive behaviour. We have demonstrated that the inclusion of small amounts of noble metal nanowires, such as Ag, can lead to a pronounced reduction in the characteristic sheet resistance of the Ni networks. Our spray-deposited networks were simple to fabricate, but the same mixing approach could be applied to other nanowire deposition methods to improve cost efficiency even further. Ag wires dominate the current flow through Ni network as evidenced in our simulations. In addition, we have introduced a novel capacitance switching model that enables the description of the activation of the networks upon electrical stimulation. The model confirms our experimental results showing that the inclusion of Ag wires onto Ni nanowire networks can lead to the reduction of the activation voltages of the samples. Nonetheless, the improvement of the network activation is not only a matter of adding additional silver wires: the positioning of the Ag wires across the network area cannot

be ignored. By taking this into consideration in our computational description, we were able to explain the observed fluctuations of the activation voltages observed in the experiments. The addition of Ag wires is particularly effective for large networks where activation voltages in a Ni-only network would be prohibitively high. These findings enable the use of co-percolative nanowire networks in a wide range of technological devices while retaining robust memristive responses at moderate voltages, enabling nanowire networks to be used for high-voltage electrostatic actuators or 'smart' neuromorphic materials.

Acknowledgements

The authors acknowledge funding from the European Research Council (ERC) under Advanced Grant 321160. This publication has emanated from research supported in part by a research grant from Science Foundation Ireland (SFI) under Grant Number SFI/12/RC/2278. The facilities and staff at the Advanced Microscopy Laboratory at Trinity College Dublin are acknowledged for their support, as is the TCHPC at Trinity College Dublin for computational resources.

References

1 S. Ye, A. R. Rathmell, Z. Chen, I. E. Stewart and B. J. Wiley, *Adv. Mater.*, 2014, **26**, 6670–87.

2 D. Langley, G. Giusti, C. Mayousse, C. Celle, D. Bellet and J.-P. Simonato, *Nanotechnology*, 2013, **24**, 452001.

3 B. Deng, P.-C. Hsu, G. Chen, B. N. Chandrashekar, L. Liao, Z. Ayitimuda, J. Wu, Y. Guo, L. Lin, Y. Zhou, M. Aisijiang, Q. Xie, Y. Cui, Z. Liu and H. Peng, *Nano Lett.*, 2015, **15**, 4206–4213.

4 X. Lan, J. Bai, S. Masala, S. M. Thon, Y. Ren, I. J. Kramer, S. Hoogland, A. Simchi, G. I. Koleilat, D. Paz-Soldan, Z. Ning, A. J. Labelle, J. Y. Kim, G. Jabbour and E. H. Sargent, *Adv. Mater.*, 2013, **25**, 1769–1773.

5 D. P. Langley, G. Giusti, M. Lagrange, R. Collins, C. Jiménez, Y. Bréchet and D. Bellet, *Sol. Energy Mater. Sol. Cells*, 2014, **125**, 318–324.

6 J. Liang, L. Li, K. Tong, Z. Ren, W. Hu, X. Niu, Y. Chen and Q. Pei, *ACS Nano*, 2014, **8**, 1590–1600.

7 I. Chang, T. Park, J. Lee, H. B. Lee, S. H. Ko and S. W. Cha, *Int. J. Hydrogen Energy*, 2016, **41**, 6013–6019.

8 I. Chang, T. Park, J. Lee, H. B. Lee, S. Ji, M. H. Lee, S. H. Ko and S. W. Cha, *Int. J. Hydrogen Energy*, 2014, **39**, 7422–7427.

9 I. Chang, T. Park, J. Lee, M. H. Lee, S. H. Ko and S. W. Cha, *J. Mater. Chem. A*, 2013, **1**, 8541.

10 C. K. Jeong, J. Lee, S. Han, J. Ryu, G. T. Hwang, D. Y. Park, J. H. Park, S. S. Lee, M. Byun, S. H. Ko and K. J. Lee, *Adv. Mater.*, 2015, **27**, 2866–2875.

11 S. Hong, H. Lee, J. Lee, J. Kwon, S. Han, Y. D. Suh, H. Cho, J. Shin, J. Yeo and S. H. Ko, *Adv. Mater.*, 2015, **27**, 4744–4751.

12 P. Lee, J. Ham, J. Lee, S. Hong, S. Han, Y. D. Suh, S. E. Lee, J. Yeo, S. S. Lee, D. Lee and S. H. Ko, *Adv. Funct. Mater.*, 2014.

13 P. Lee, J. Lee, H. Lee, J. Yeo, S. Hong, K. H. Nam, D. Lee, S. S. Lee and S. H. Ko, *Adv. Mater.*, 2012, **24**, 3326–3332.

14 H. Lee, S. Hong, J. Lee, Y. D. Suh, J. Kwon, H. Moon, H. Kim, J. Yeo and S. H. Ko, *ACS Appl. Mater. Interfaces*, 2016, **8**, 15449–15458.

15 K. K. Kim, S. Hong, H. M. Cho, J. Lee, Y. D. Suh, J. Ham and S. H. Ko, *Nano Lett.*, 2015, **15**, 5240–5247.

16 K. Takei, T. Takahashi, J. C. Ho, H. Ko, A. G. Gillies, P. W. Leu, R. S. Fearing and A. Javey, *Nat. Mater.*, 2010, **9**, 821–6.

17 J. Wang, J. Jiu, T. Araki, M. Nogi, T. Sugahara, S. Nagao, H. Koga, P. He and K. Suganuma, *Nano-Micro Lett.*, 2014, **7**, 51–58.

18 P. N. Nirmalraj, A. T. Bellew, A. P. Bell, J. a. Fairfield, E. K. McCarthy, C. O'Kelly, L. F. C. Pereira, S. Sorel, D. Morosan, J. N. Coleman, M. S. Ferreira and J. J. Boland, *Nano Lett.*, 2012, **12**, 5966–71.

19 V. Scardaci, R. Coull, P. E. Lyons, D. Rickard and J. N. Coleman, *Small*, 2011, **7**, 2621–2628.

20 S. Zhu, Y. Gao, B. Hu, J. Li, J. Su, Z. Fan and J. Zhou, *Nanotechnology*, 2013, **24**, 335202.

21 T. Ackermann, S. Sahakalkan, I. Kolaric, E. Westkämper and S. Roth, *Nanoeng. Fabr. Prop. Opt. Devices XII*, 2015, **9556**, 955602.

22 B. Li, S. Ye, I. E. Stewart, S. Alvarez and B. J. Wiley, *Nano Lett.*, 2015, **15**, 6722–6726.

23 A. T. Bellew, A. P. Bell, E. K. McCarthy, J. A. Fairfield and J. J. Boland, *Nanoscale*, 2014, **6**, 1–3.

24 D. B. Strukov, G. S. Snider, D. R. Stewart and R. S. Williams, *Nature*, 2008, **453**, 80–83.

25 J. A. Fairfield, C. Ritter, A. T. Bellew, E. K. McCarthy, M. S. Ferreira and J. J. Boland, *ACS Nano*, 2014, **8**, 9542–9549.

26 S. De, T. M. Higgins, P. E. Lyons, E. M. Doherty, P. N. Nirmalraj, W. J. Blau, J. J. Boland and J. N. Coleman, *ACS Nano*, 2009, **3**, 1767–1774.

27 E. C. Garnett, W. Cai, J. J. Cha, F. Mahmood, S. T. Connor, M. Greyson Christoforo, Y. Cui, M. D. McGehee and M. L. Brongersma, *Nat. Mater.*, 2012, **11**, 241–249.

28 A. P. Bell, J. A. Fairfield, E. K. McCarthy, S. Mills, J. J. Boland, G. Baffou and D. McCloskey, *ACS Nano*, 2015, **9**, 5551–5558.

29 L. Hu, H. S. Kim, J.-Y. Lee, P. Peumans and Y. Cui, *ACS Nano*, 2010, **4**, 2955–2963.

30 S. La Barbera, D. Vuillaume and F. Alibart, *ACS Nano*, 2015, **9**, 941–9.

31 S. R. Das, S. Sadeque, C. Jeong, R. Chen, M. A. Alam and D. B. Janes, *Nanophotonics*, 2016, **5**, 180–195.

32 T. Ackermann, S. Sahakalkan, I. Kolaric, E. Westkämper and S. Roth, *Phys. status solidi - Rapid Res. Lett.*, 2015, **9**, 141–144.

33 T. Tokuno, M. Nogi, J. Jiu and K. Suganuma, *Nanoscale Res. Lett.*, 2012, **7**, 281.

34 J. S. Woo, J. T. Han, S. Jung, J. I. Jang, H. Y. Kim, H. J. Jeong, S. Y. Jeong, K.-J. Baeg and G.-W. Lee, *Sci. Rep.*, 2014, **4**, 4804.

35 A. R. Rathmell, M. Nguyen, M. Chi and B. J. Wiley, *Nano Lett.*, 2012, **12**, 3193–3199.

36 I. E. Stewart, A. R. Rathmell, L. Yan, S. Ye, P. F. Flowers, W. You and B. J. Wiley, *Nanoscale*, 2014, **6**, 5980–8.

37 S. M. Bergin, Y.-H. Chen, A. R. Rathmell, P. Charbonneau, Z.-Y. Li and B. J. Wiley, *Nanoscale*, 2012, **4**, 1996.

38 R. Waser and M. Aono, *Nat. Mater.*, 2007, **6**, 833–840.

39 J. Joshua Yang, F. Miao, M. D. Pickett, D. a a Ohlberg, D. R. Stewart, C. N. Lau and R. S. Williams, *Nanotechnology*,

2009, **20**, 215201.
40 S. M. Oliver, J. A. Fairfield, A. T. Bellew, S. Lee, J. Champlain, L. B. Ruppalt, J. J. Boland and P. M. Vora, *submitted*.
41 C. Gomes da Rocha, H. G. Manning, C. O'Callaghan, C. Ritter, A. T. Bellew, J. J. Boland and M. S. Ferreira, *Nanoscale*, 2015, **7**, 13011–6.
42 R. M. Mutiso and K. I. Winey, *Phys. Rev. E - Stat. Nonlinear, Soft Matter Phys.*, 2013, **88**.
43 R. M. Mutiso, M. C. Sherrott, A. R. Rathmell, B. J. Wiley and K. I. Winey, *ACS Nano*, 2013, **7**, 7654–7663.
44 S. Kirkpatrick, *Rev. Mod. Phys.*, 1973, **45**, 574–588.
45 A. T. Bellew, H. G. Manning, C. Gomes da Rocha, M. S. Ferreira and J. J. Boland, *ACS Nano*, 2015, **9**, 11422–11429.
46 J. Li and S. L. Zhang, *Phys. Rev. E - Stat. Nonlinear, Soft Matter Phys.*, 2009, **80**.
47 T. Watanabe and A. Nakamura, *J. Comput. Syst. Sci.*, 1987, **35**, 96–144.
48 S. Khuller and R. Thurimella, in *Lecture Notes in Computer Science, Volume 623*, 1992, pp. 330–341.

1

Supporting Information for "Co-percolation To Tune Conductive Behaviour in Dynamical Metallic Nanowire Networks"

J. A. Fairfield[a,c,†], C. G. Rocha[b,c], C. O'Callaghan[b,c], M. S. Ferreira[b,c] and J. J. Boland[a,c,*]

[a.] *School of Chemistry, Trinity College Dublin, Dublin 2, Ireland.*
[b.] *School of Physics, Trinity College Dublin, Dublin 2, Ireland.*
[c.] *Centre for Research on Adaptive Nanostructures and Nanodevices (CRANN), Trinity College Dublin, Dublin 2, Ireland.*
†Present address: School of Physics, National University of Ireland Galway, University Road, Galway, Ireland.

1. Nanowire Density in Networks Measured Experimentally

TABLE SI. Nanowire densities for experimental nanowire networks of varying compositions of Ni/Ag.

Nanowire composition Ni/Ag	Nanowire density (NW/μm^2)
100/0	0.22
93/7	0.25
85/15	0.19
70/30	0.30
68/32	0.24

2. Arithmetic versus Geometric Mean for Ni-Ag Nanowire Junctions

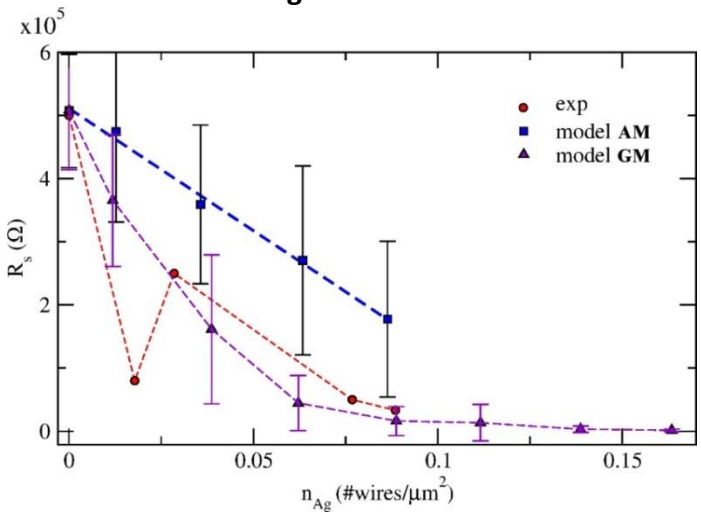

Figure S1. Sheet resistance (R_s) versus Ag wire density (n_{Ag}) calculated for nanowire networks with a total wire density of n = 0.25 nanowires/μm^2. Results are shown considering that the hybrid junction resistance R_j^{NA} is written in terms of (squares) an arithmetic mean (AM) or (triangles) a geometric mean (GM) of R_j^{NN} and R_j^{AA}. Circles correspond to measured values. The experimental sample has dimensions of 100 x 100 μm.

Figure S1 shows how the calculated sheet resistances compare with the experimental values as the concentration of Ag nanowires increases. Simulations were performed considering that the hybrid Ni-Ag junctions are modelled within arithmetic mean (AM) or geometric mean (GM) representation. As a result of their better conducting attributes, Ag nanowires tend to lower the sheet resistance of Ni nanowire networks as evidenced by experiment. More importantly, the reduction is substantial and it can be achieved with relatively small concentrations of Ag wires. The decrease in R_s is non-linear and its trend is completely captured by our numerical description following GM representation. On the other hand, AM scheme predicts a spurious linear dependency between R_s and n_{Ag}. Therefore, it is clear that GM enables a meaningful evaluation of the transport properties of hybrid nanowire networks. For sets of highly discrepant values such as the experimental nanowire junction resistances, GM dampens the influence of the highest numbers providing less biased, more accurate results for the calculated averages.

3. Dynamical activation of Ni/Ag nanowire networks

The files c6nr06276h3.mpg, c6nr06276h2.mpg, and c6nr06276h1.mpg show the full dynamical activation of a pristine Ni NWN sample and hybrid ones with Ni/Ag = 95/5%, and Ni/Ag = 75/25%, respectively. Stars indicate junctions that were activated at each simulation step. Charge is loaded on the electrodes until a path of activated junctions bridges them. All wires composing this path are highlighted in blue at the end of the animation. FIG S2 shows some snapshots of the corresponding animations.

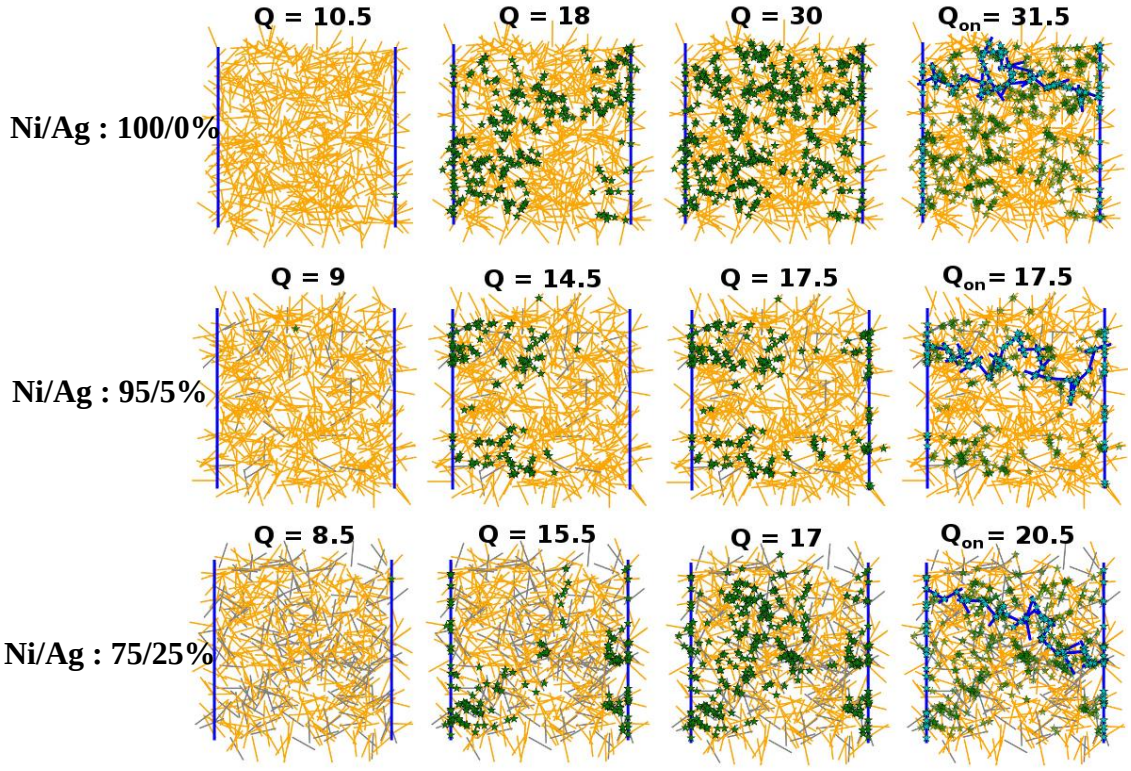

Figure S2. Snapshots of the dynamical activation of a (upper panels) pure Ni nanowire network, and hybrid networks containing Ni/Ag fractions of (middle panels) 95/5% and (lower panels) 75/25%. Green stars represent junctions that were activated to its ON-state as charge (Q) is loaded into the electrodes. Eventually a path of ON-state junctions bridges the electrodes (blue path) evidencing that current can finally flow through it. The amount of charge required to enable this path is given by Q_{on} specified in terms of arbitrary units. All networks have fixed density of n = 0.25 nanowires/μm^2 and dimensions 50 x 50 μm.

4. Activation of Ni/Ag nanowire networks: increasing capacitance contrast

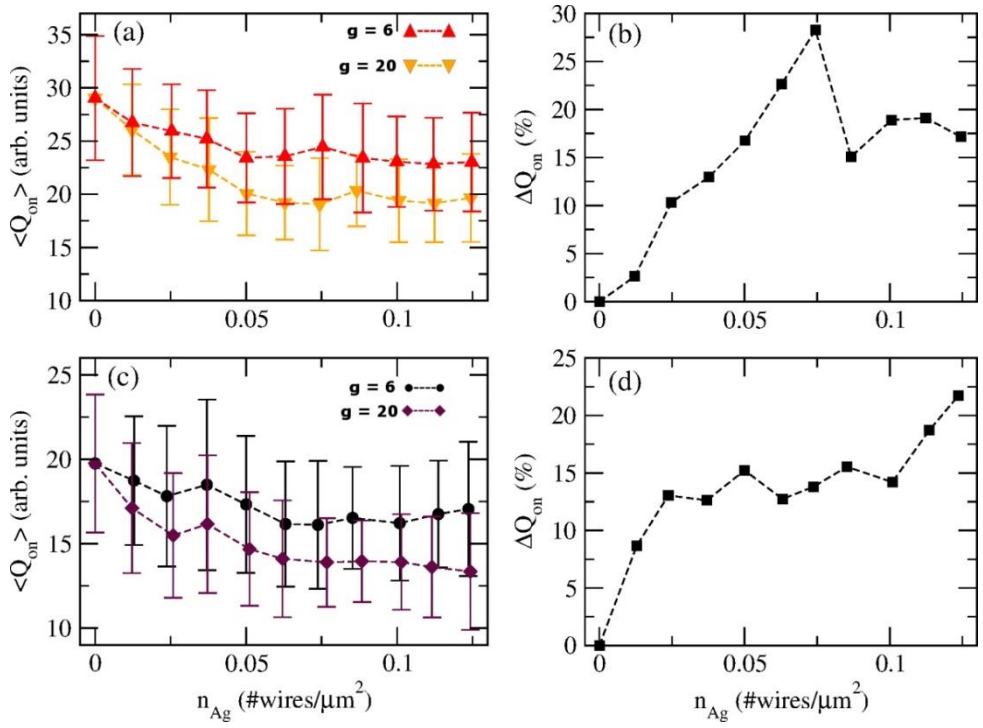

Figure S3. (Left panels) Average amount of charge required to establish a percolative path of activated junctions (<Q_{on}>) on Ni/Ag nanowire networks as a function of Ag wire density (n_{Ag}) for (a) d = 50 μm and (c) d = 35 μm. Each data point is a result of statistical ensembles containing 50 representative networks of sizes d x d and fixed wire density of n = 0.25 nanowires/μm^2. The parameter g is the proportionality constant which defines the capacitance contrast of the wires, i.e. $\boldsymbol{C^{OFF}(Ag) = gC^{OFF}(Ni)}$. (Right panels) Percent relative error in <Q_{on}> taken from the curves g = 6 and g = 20 on the left panels (ΔQ_{on}) as a function of n_{Ag}. Panel (b) corresponds to the case where d = 50 μm whereas (d) corresponds to d = 35 μm.